3607

CARLOS

LA-10927-MS

UC-70
Issued: April 1987

Minerals in Fractures of the Saturated Zone from Drill Core USW G-4, Yucca Mountain, Nye County, Nevada

B. Arney Carlos

Los Alamos National Laboratory
Los Alamos, New Mexico 87545

CONTENTS

FIGURES

MINERALS IN FRACTURES OF THE SATURATED ZONE FROM DRILL CORE USW G-4, YUCCA MOUNTAIN, NYE COUNTY, NEVADA

by

B. Arney Carlos

ABSTRACT

The minerals in fractures in drill core USW G-4, from the static water level (SWL) at 1770 ft to the base of the hole at 3000 ft, were studied to determine their identity and depositional sequence and to compare them with those found above the SWL in the same drill hole. There is no change in mineralogy or mineral morphology across the SWL. The significant change in mineralogy and relationship to the host rock occurs at 1381 ft, well above the present water table. Below 1381 ft clinoptilolite appears in the fractures and rock matrix instead of heulandite, and the fracture mineralogy correlates with the host rock mineralogy. Throughout most of the saturated zone (below the SWL) in USW G-4, zeolites occur in fractures only in zeolitic tuff; however, zeolites persist in fractures below the base of the deepest zeolitic tuff interval. The zeolites are mordenite and clinoptilolite in both fractures and zeolitic matrix, but mordenite is more abundant in fractures and clinoptilolite predominates in the matrix. Clinoptilolite larger than 0.05 mm is rare in fractures. Nonzeolitic intervals of tuff have fewer fractures, and many of these have no coatings; a few have quartz and feldspar coatings. One interval in zeolitic tuff (2125-2140 ft) contains abundant cristobalite coatings in the fractures. Calcite occurs in fractures from 2575 to 2660 ft, usually with the manganese mineral hollandite, and from 2750 to 2765 ft, usually alone. Manganese minerals occur in several intervals. Most are hollandite or cryptomelane, but pyrolusite also occurs in the shallower intervals. The manganese minerals may occur with zeolites, quartz, or calcite and often line the fractures beneath other minerals, but they also may occur later in the paragenetic sequence. Two or more manganese minerals or different compositions of hollandite in the same fracture are not unusual. The spatial correlation of zeolites in fractures with zeolitic host rock suggests that both may have been zeolitized at the same time, possibly by water moving laterally through more permeable zones in the tuff. The continuation of zeolites in fractures below the lowest zeolitic interval in this hole suggests that vertical fracture flow may have been important in the deposition of these coatings. Core from deeper intervals in another hole will be examined to determine if that relationship continues.

I. INTRODUCTION

Yucca Mountain, located on the southwest margin of the Nevada Test Site (Fig. 1), is being studied as a potential repository for high-level nuclear waste. These studies are coordinated under the Nevada Nuclear Waste Storage Investigations (NNWSI) Project managed by the Nevada Operations Office of the US Department of Energy. Detailed descriptions of the ash flow tuffs underlying the mountain are given in Lipman et al. (1966), Byers et al. (1976), and Carr et al. (1986). Quantitative x-ray diffraction (XRD) data on the mineralogy of the tuffs in several drill holes at Yucca Mountain and cross sections showing distribution of these minerals are presented in Bish and Vaniman (1985). Stress regimes, regional structure, and fracture abundance and orientation have been discussed by Carr (1974) and by Scott et al. (1983). The importance of fractures as groundwater flow paths, especially through densely welded tuff, was emphasized by Scott et al. (1983), who presented a hydrologic model for fluid flow in the unsaturated zone of Yucca Mountain.

Understanding natural barriers to radionuclide migration is important in evaluating a potential waste repository site. Studies of sorptive minerals such as clays, zeolites, and manganese oxides along flow paths away from the repository site must include the minerals that line fractures as well as those in the rock matrix. Studying fracture mineralogy and the similarities and differences between fracture and rock-matrix mineralogy could also provide information about rock-alteration histories and paleo water tables. Alteration histories can be used to predict what might happen in the thermal regime produced by the waste after it is emplaced.

Several holes have been drilled in Yucca Mountain for geologic and hydrologic studies. Drill hole USW G-4, the most recent cored hole within the prospective repository block, was chosen for detailed study of fracture-lining minerals because it is closest to the planned NNWSI exploratory shaft. A study of the fracture minerals in USW G-4 drill core should indicate conditions that can be expected along flow paths within the northeastern part of the repository.

Drill hole USW G-4 was drilled in 1982 and continuously cored from 22 ft to 3001 ft total depth (TD). The drilling history, core lithology, and geophysical logs of the well are given in Spengler et al. (1984). Stratigraphic descriptions used in this report are from Spengler et al. (1984). A preliminary study of frequency and orientation of fractures in the core is

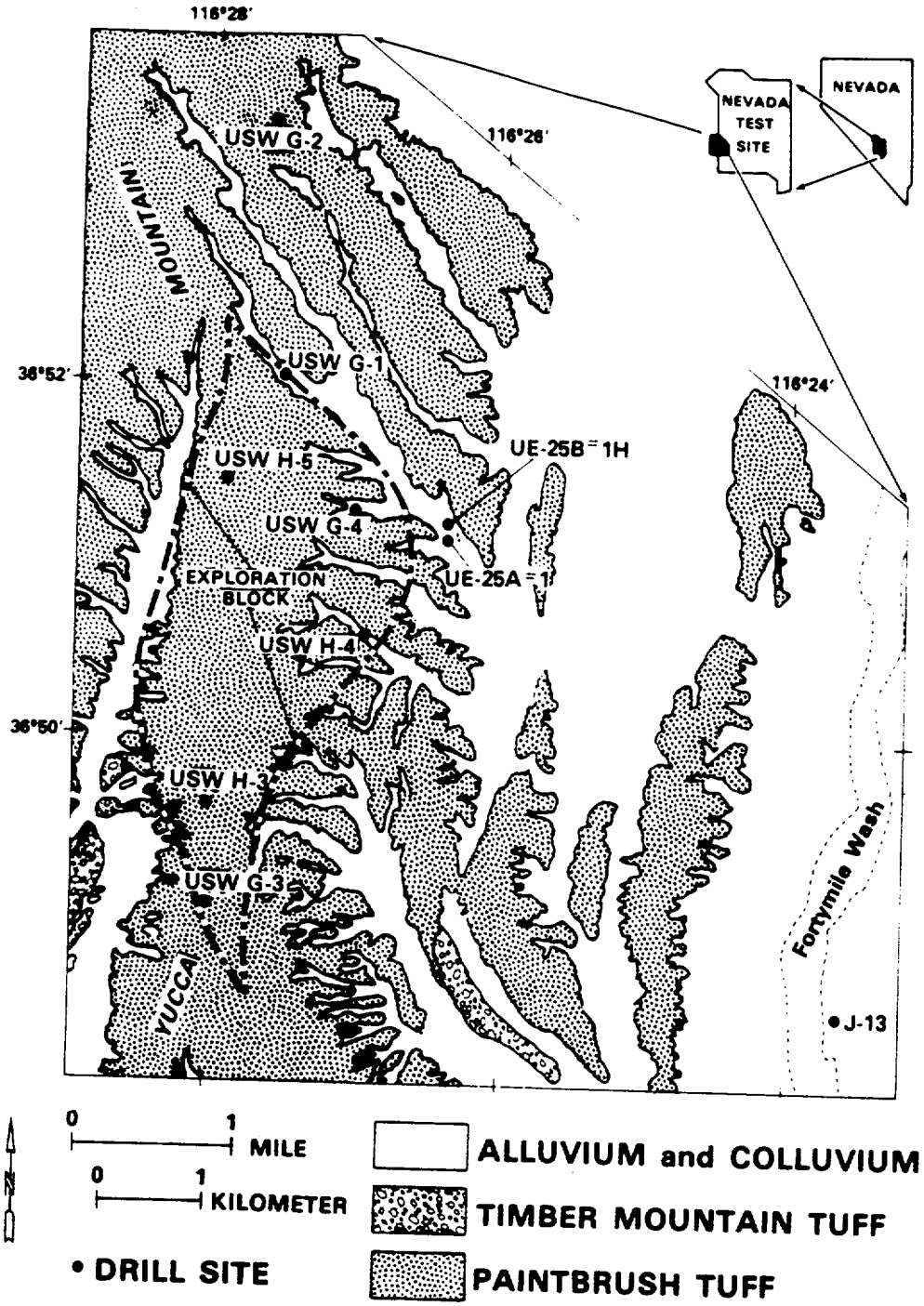

Fig. 1.
Location map showing Yucca Mountain and drill holes.

included in Spengler et al. (1984); a more detailed study is being performed by the US Geological Survey with the help of geologists from Fenix & Scisson. No attempt has been made in this study to quantify the relative abundances of different fracture types. Fracture mineralogy in the unsaturated zone [above the static water level (SWL)] in USW G-4 has been described in Carlos (1985).

A general stratigraphy of USW G-4 below the SWL based on Spengler et al. (1984) is shown in Fig. 2. Some of the breaks between zeolitic and non-zeolitic intervals have been modified slightly by XRD studies (Bish and Vaniman 1985; Chipera, written commun., 1986). The depth of the SWL is 1770 ft.* The total depth penetrated by USW G-4 below the SWL is entirely within the Crater Flat Tuff. There are three zeolitic intervals in this unit in USW G-4. They are stratigraphically defined in that they occur at the originally nonwelded tops and bottoms of flow units, but there is no break either across members of the Crater Flat Tuff or between the Crater Flat Tuff and the overlying Tuffs of Calico Hills; the top of one Member and the base of the overlying Member form one zeolitic interval (Broxton and Carlos 1986). All three zeolitic intervals are within the clinoptilolite-mordenite alteration zone.

II. METHODS

Representative core samples for each interval and each fracture type within an interval were selected for study. Samples with the most extensive coatings for each type of fracture were chosen to provide sufficient material for XRD analysis; therefore, estimating the mineral abundances in all fractures based on the surface coverage listed in Table I for the selected samples will give invalid results. All samples were first examined using a binocular microscope (50x magnification). At 50x, crystals $\geq$0.02 mm can be clearly distinguished. Coatings with crystals of this size are therefore described as microcrystalline. Crystals $\leq$0.01 mm cannot be distinguished at 50x, and coatings of this size are described as cryptocrystalline. Representative samples were chosen for scanning electron microscope (SEM) analysis. Samples for XRD were scraped from fracture surfaces with a steel scraper, and the scraped fragments were hand-picked under the binocular microscope. The

* Information provided by J. Robison, US Geological Survey (May 22, 1984).

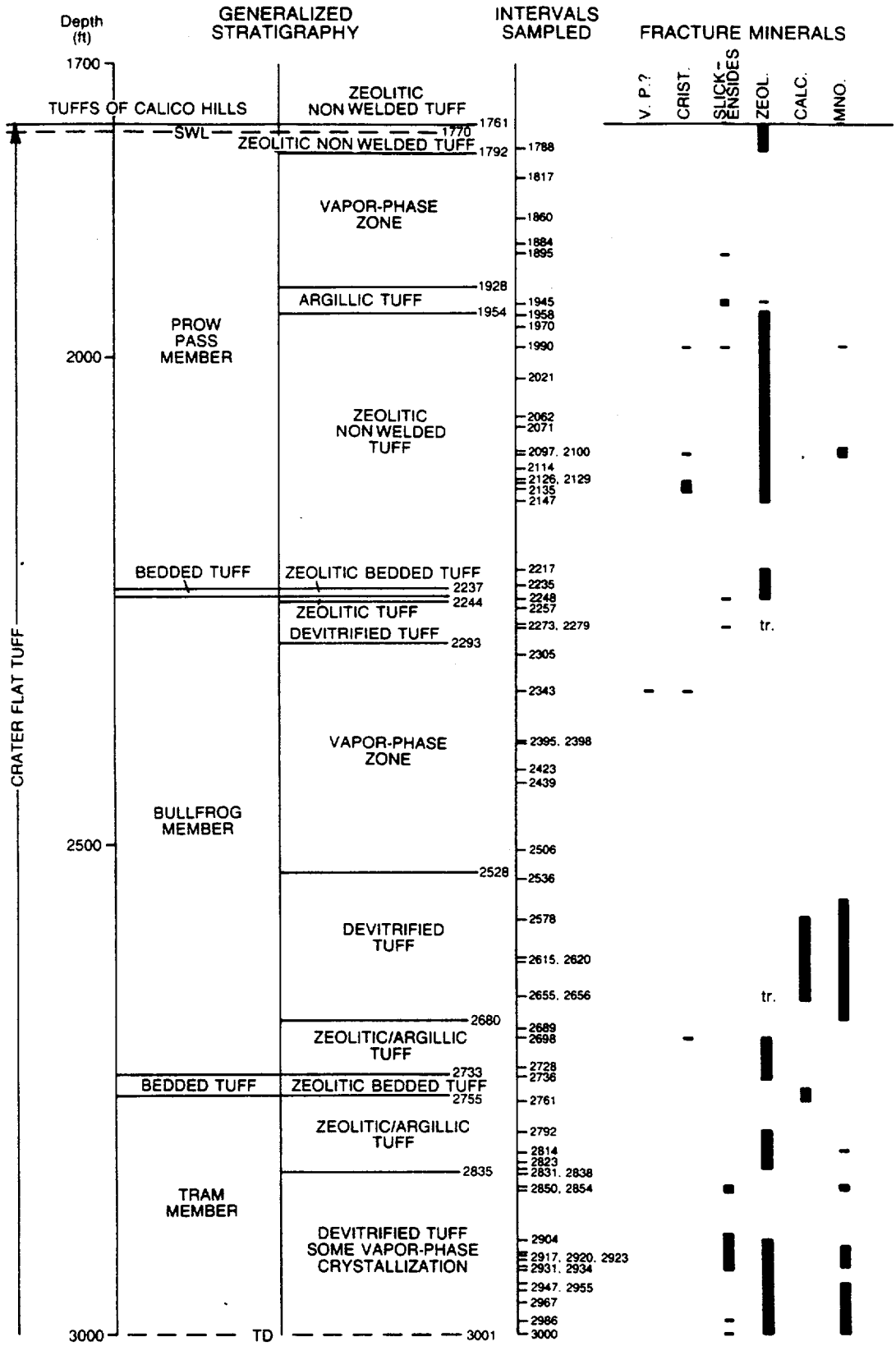

Fig. 2.
Generalized stratigraphy, modified from Spengler et al. (1984), intervals sampled and fracture minerals in the saturated zone of USW G-4.

maximum amount of contamination from the rock matrix was estimated on the basis of visual inspection of the scraped material after hand-picking and the apparent ease of separating coating from matrix during scraping. The samples were then crushed to powder in a ceramic mortar and exposed to x rays either as pressed-powder or as water-smear samples, depending on the amount of material available. XRD patterns were obtained in the step-scan mode with a Siemens D-500 powder diffractometer using a copper-target x-ray tube and a diffracted-beam monochromator. Because of the different amounts of sample obtainable from each fracture, the times at each step were adjusted to give acceptable signal-to-noise ratios. Some samples that gave questionable results at shorter scan rates or that apparently contained substantial amounts of manganese minerals were run overnight at a scan rate of 12 min/deg (2θ); other samples were analyzed at between 1.6 and 4.2 min/deg.

Mineral identifications were made by comparing observed patterns with standard patterns produced by this XRD system and by comparing patterns with standards from the Joint Committee on Powder Diffraction Standards (JCPDS). JCPDS card numbers and the characteristic peaks of minerals found in Yucca Mountain tuffs were reported by Bish et al. (1981). The mineral concentrations were estimated by comparing peak intensities of the unknown samples with in-lab standard patterns of known mixtures as described in Bish and Vaniman (1985). As outlined in that report, several assumptions are implicit in such estimates, including an assumed lack of significant preferred orientation and of appreciable variations in intensity with compositional changes. Small amounts of sample available from fractures required the use of water-smear samples or (rarely) small-cavity glass slides rather than the larger-cavity glass slides. Particles were unavoidably oriented during this process. In addition, low-angle intensities are too low relative to higher-angle peaks when small smear mounts are used. Minor intensity humps in the XRD patterns of several samples resulted from x rays reflecting off the glass slide. Estimating intensity of XRD peaks from such samples is difficult. Overlapping XRD peaks of the several minerals in each sample cause additional problems in any attempt to quantify the XRD results of these samples. Mordenite and clinoptilolite are common in these samples and introduce sizable uncertainties in the quantification of the feldspars especially. Because the extent of orientation of the mineral grains was unknown, it was

TABLE I

SEMIQUANTITATIVE X-RAY DIFFRACTION ANALYSES OF FRACTURE FILLINGS IN USW G-4, SATURATED ZONE

Sample (ft) Depth	Est. Fract Coverage %	Est. Max % Contamination	Smectite	Clinoptilolite	Mordenite	Quartz	Cristobalite	AF	Other
1788	95	2	--	--	100	--	--	--	--
1970	Not readily discernible from rock matrix		--	10	80	10	--	--	--
1991 orange	70	20	tr	10	30	10	tr	50	--
1991 black*	Not determined, intergrown with rock grains		10	30	50	10	--	--	--
2062	60	10	--	20	75	5	--	--	--
2071	80	30	--	20	60	20	--	--	--
2099*	95	3	--	95	tr	tr	5	--	--
2100 horiz*	85	10	--	90	--	10	--	--	--
2100 white	80	5	--	5	95	tr	--	--	--
2101 white	95	1	--	10	90	tr	--	--	--
2101 beige	95	1	--	10	75	5	--	10	--
2135	100	5	--	--	--	--	100	--	--
2147 white	90	15	--	50	50	tr	--	--	--
2147 pink	95	10	--	15	75	5	--	5	--
2248	90	15	--	40	40	tr	--	20	--
2344	95	20	--	--	--	70	tr	30	--
2578*	100	20	--	--	--	60	tr	10	30[a]
2615*	95	7	--	--	--	30	--	70	--
2689	Not readily discernible from rock matrix		40	--	--	40	--	20	--
2698	100	5	--	60	30	--	10	--	--
2728	90	10	--	tr	100	tr	--	--	--
2793	100	2	--	90	10	--	--	--	--
2823	100	1	5	5	80	10	--	--	--
2832	98	5	20	20	50	10	--	--	--
2854*	Not determined, intergrown with rock matrix		--	--	--	40	--	60	tr[b]
2931	30	10	40	--	20	40	--	--	--
2947	100	5	--	--	--	100	--	--	--
2955*	85	15	--	--	--	40	--	60	--
2967*	90	5	--	--	--	60	--	40	--
2985	90	10	--	--	--	100	--	tr	--

* Sample contains manganese oxides. Percentages are relative for other minerals in sample, and no estimate of actual abundances has been attempted.

[a] Calcite.

[b] Mica.

difficult to correct for peak overlaps. In spite of the difficulties introduced by the sample preparation method and the overlap of peaks used in the quantitative program, it was still deemed useful to put semiquantitative values on the amounts of different minerals present. The results presented in Table I are therefore semiquantitative rather than quantitative results, as described in Bish and Vaniman (1985), and the numbers should be considered ±25% of their value (e.g., 10 ± 2.5).

Manganese minerals were identified by comparing observed patterns with standards from JCPDS and with published XRD patterns for these manganese minerals. As no in-house standard mixtures yet exist for these minerals, the relative abundances of manganese minerals could not be determined, and the abundances given in Table I for samples containing manganese oxides are normalized to 100% exclusive of the manganese minerals. In some cases manganese oxides are more than half of the total fracture coating.

Thin sections of samples that had sealed fractures were made for microprobe analysis. Making thin sections across most open fractures was impossible because of differential grinding of the softer fracture-filling minerals. Elemental compositions of minerals were determined on an automated Cameca electron microprobe with accelerating potential fixed at 15 kV and a sample current of 15 μA on thorium oxide. Analyses were made at either 20 s or 30,000 counts for each element. Compositions were calculated from corrected peak intensities using the methods of Bence and Albee (1968). Feldspar standards were used for the zeolite analyses. The Bence-Albee corrections are thus based on a dense, anhydrous tectosilicate structure (feldspar) with assumed absorption/fluorescence of the returning x rays from the sample based on that structure. The zeolite structure contains considerable void space that is normally filled with water that vaporizes during the analysis. For this reason, zeolite analyses using feldspar standards and Bence-Albee corrections not only have low totals but also may yield cation ratios that are not as accurate as those for most anhydrous silicates. Some sodium migration (Graham et al. 1984) was unavoidable. Because crystals were small, a small raster had to be used, and the beam often could not be moved to new areas of the crystal during analysis. Therefore, most of the analyses probably indicate slightly less sodium than is actually present. Zeolite analyses given in Table II and cation ratios shown in Fig. 9 should be used only to compare analyses obtained by this method. They are not necessarily as

accurate as analyses made by other methods. Microprobe analyses of manganese minerals (Table III) were performed under the same operating conditions as zeolite analyses. Oxide mineral standards rather than silicates or sulfides were used for most elements. In addition to the elements listed in Table III, W, Cu, and Pb were looked for but not seen on the energy-dispersive spectra taken concurrently with the wavelength dispersive analysis. Because of the Ce overlap problems with Ba, Ce could not be measured directly. Instead the Ce $L\alpha 1+2$ combined peak (which overlaps with the Ba $L\beta 1$ peak) was counted and a calibration curve developed for apparent counts per second (cps) minus background/% measured BaO. Standards containing Ce were also measured to determine cps/% Ce. Only one manganese oxide sample had higher counts for the Ce peak than would be expected for the amount of Ba present. A better calibration curve would be required to determine the actual amount of Ce present. Manganese minerals were often intergrown with silica or zeolites and, in one sample, with calcite. Areas of highest reflectance generally gave the best (least contaminated) results. Most samples had at least a few spots where the manganese oxides were dense enough to give reasonable totals and stoichiometry for that mineral (Table III). A few have low totals and this is attributed to the acicular form of the mineral and epoxy-filled void space between individual grains. Very few samples contained crystals large enough that an analysis could be done on a single crystal.

Imaging and qualitative composition studies were made on an ISI model DS-130 scanning electron microscope, operated between 15 and 40 keV. Qualitative analyses from primary x-ray signals were obtained on a Kevex model 7000 energy-dispersive system with the electron beam operating at 15 and 19 keV. The SEM photographs used in this report are of secondary-electron images.

III. DESCRIPTIONS OF FRACTURE-LINING SILICATES

The silicate minerals that line fractures below the SWL in USW G-4 can be divided into four groups: the zeolites mordenite and clinoptilolite, the silica minerals quartz and cristobalite, feldspar, and a few occurrences of smectite clays.

Unlike zeolites in fractures above the SWL in USW G-4 (Carlos 1985), the occurrence of zeolites in fractures below the SWL correlates closely with zeolitic and argillic intervals in the tuff (Fig. 2). There are essentially three intervals of zeolitic fracture fill in the saturated zone; though

TABLE II

REPRESENTATIVE COMPOSITIONS OF ZEOLITES BELOW THE SWL IN DRILL HOLE USW G-4

	Clinoptilolite at 2099 ft				Clinoptilolite at 2100 ft				
	Large Euhedral Crystals		Earlier Crystals		Fracture Rim	Large Euhedral		Small Fracture	3rd Fracture
SiO_2	66.8	66.8	69.0	66.4	60.9	67.8	68.3	69.7	68.1
TiO_2	0.02	0.01	0.01	0.03	0.02	0.05	0.02	0.05	0.03
Al_2O_3	11.6	11.8	12.8	12.3	10.9	12.2	12.7	12.7	12.5
Fe_2O_3	0.00	0.06	0.00	0.01	0.00	0.08	0.02	0.03	0.09
MgO	0.06	0.07	0.08	0.11	0.09	0.06	0.10	0.10	0.12
CaO	3.43	3.53	3.70	3.75	2.94	3.32	3.62	3.53	3.43
BaO	0.00	0.00	0.00	0.00	0.00	0.00	0.03	0.12	0.10
Na_2O	1.33	1.15	1.31	0.84	1.24	1.09	1.01	1.21	0.97
K_2O	2.34	2.16	2.21	2.34	2.41	2.65	2.68	2.51	2.91
Total	85.6	85.6	89.1	85.8	78.5	87.2	88.5	90.0	88.3
Unit-Cell Composition Based on 72 (O)									
Si	29.9	29.9	29.7	29.7	29.8	29.8	29.7	29.7	29.7
Ti	0.01	0.00	0.00	0.01	0.01	0.02	0.01	0.02	0.01
Al	6.12	6.24	6.47	6.49	6.31	6.31	6.49	6.40	6.44
Fe	0.00	0.02	0.00	0.00	0.00	0.03	0.01	0.01	0.03
Mg	0.04	0.05	0.05	0.07	0.07	0.04	0.06	0.06	0.08
Ca	1.65	1.69	1.70	1.80	1.54	1.57	1.68	1.61	1.60
Ba	0.00	0.00	0.00	0.00	0.00	0.00	0.01	0.02	0.02
Na	1.16	1.00	1.09	0.73	1.18	0.93	0.85	1.00	0.82
K	1.34	1.23	1.21	1.33	1.50	1.49	1.48	1.37	1.62
Si/(Al+Fe)	4.90	4.77	4.59	4.57	4.72	4.70	4.57	4.64	4.59
(Al+Fe)/(2Mg+2Ca+2Ba+Na+K)	1.04	1.10	1.11	1.12	1.07	1.13	1.11	1.11	1.11
Mol.% Exchangeable Cations									
K	32.0	31.1	29.9	33.9	35.1	37.0	36.4	33.8	39.3
Na	27.6	25.1	26.9	18.5	27.4	23.1	20.8	24.7	19.9
Ca+Mg	40.4	43.8	43.2	47.5	37.5	39.9	42.8	41.5	40.8

TABLE II (cont)

	Zeolites at 2698 ft					
	Euhedral Clinoptilolite				Mordenite	
SiO_2	70.2	71.7	71.7	71.1	75.8	76.3
TiO_2	0.03	0.00	0.01	0.00	0.00	0.02
Al_2O_3	13.8	13.6	13.5	13.7	11.7	12.0
Fe_2O_3	0.00	0.03	0.00	0.00	0.01	0.00
MgO	0.17	0.21	0.23	0.26	0.01	0.00
CaO	4.85	4.48	4.56	4.79	3.52	3.46
BaO	0.00	0.02	0.00	0.00	0.06	0.00
Na_2O	1.66	1.82	1.49	1.49	2.06	2.09
K_2O	0.94	1.20	1.12	1.33	0.56	0.67
Total	91.6	93.1	92.6	92.6	93.7	94.5
Unit-Cell Composition Based on 72 (O)						
Si	29.3	29.5	29.6	29.4	30.6	30.5
Ti	0.01	0.00	0.00	0.00	0.00	0.01
Al	6.80	6.60	6.56	6.67	5.57	5.65
Fe	0.00	0.01	0.00	0.00	0.00	0.00
Mg	0.11	0.13	0.14	0.16	0.01	0.00
Ca	2.17	1.97	2.01	2.12	1.52	1.48
Ba	0.00	0.00	0.00	0.00	0.01	0.00
Na	1.34	1.45	1.19	1.19	1.61	1.62
K	0.50	0.63	0.59	0.70	0.29	0.34
Si/(Al+Fe)	4.31	4.46	4.51	4.41	5.49	5.41
(Al+Fe)/(2Mg+2Ca+2Ba+Na+K)	1.06	1.05	1.08	1.03	1.12	1.15
Mol.% Exchangeable Cations						
K	12.2	15.0	15.0	16.8	8.4	9.9
Na	32.6	34.7	30.3	28.6	47.0	47.0
Ca+Mg	55.2	50.3	54.8	54.6	44.6	43.0

TABLE III

REPRESENTATIVE MICROPROBE ANALYSES OF MANGANESE MINERALS IN FRACTURES

	Pyrolusite 1991	Hollandite 1991		Pyrolusite 2099	Hollandite 2099		Cryptomelane 2615	Ferrian Hollandite 2620	Ferrian Hollandite 2656	
SiO_2	5.22	0.24	0.55	0.80	0.33	0.35	0.58	0.72	1.23	0.57
TiO_2	0.20	0.09	n.d.	n.d.	0.16	0.13	0.38	1.64	2.03	0.69
MnO_2	84.47	87.13	84.12	78.28	78.70	78.11	66.40	75.39	69.55	77.72
Al_2O_3	1.34	0.46	0.34	0.13	0.30	0.42	0.24	0.67	0.54	0.47
Fe_2O_3	3.15	0.83	1.03	1.37	1.92	1.24	2.51	7.06	7.32	4.17
MgO	0.10	n.d.	n.d.	n.d.	0.31	n.d.	0.29	0.14	1.78	2.91
CaO	0.38	0.11	0.14	0.07	0.06	0.15	1.86	0.22	1.28	1.42
BaO	0.18	5.05	8.62	2.12	14.26	12.07	2.75	7.80	3.16	2.30
SrO	0.44	0.19	0.11	0.45	0.19	0.15	1.79	3.22	0.85	0.60
K_2O	0.18	4.65	2.91	0.08	0.54	1.22	0.92	1.40	0.57	0.16
Na_2O	0.20	0.23	0.33	0.10	0.13	0.13	1.30	0.54	1.56	2.02
CeO_2	n.d.	n.d.	n.d.	n.d.	n.d.	n.d.	n.d.	n.d.	n.d.	n.d.
ZnO	0.22	n.d.	n.d.	0.56	0.20	n.d.	0.34	0.08	0.24	0.18
NiO	0.26	n.d.	n.d.	0.34	0.29	n.d.	n.d.	0.10	n.d.	n.d.
Total	96.34	98.98	98.15	84.30	97.39	93.97	79.36	98.98	90.11	93.21
	Stoich (O=2)	Stoich (O=16)	Stoich (O=16)	Stoich (O=2)	Stoich (O=16)	Stoich (O=16)	Stoich (O=16)	Stoich (O=16)	Stoich (O=16)	Stoich (O=16)
Si	0.08	0.03	0.07	0.02	0.04	0.05	0.09	0.09	0.17	0.07
Ti	-	0.01	-	-	0.02	0.01	0.04	0.16	0.21	0.07
Mn	0.87	7.51	7.44	0.95	7.28	7.39	7.10	6.71	6.48	6.91
Al	0.02	0.07	0.05	-	0.05	0.07	0.04	0.10	0.09	0.07
Fe	0.04	0.08	0.10	0.02	0.19	0.13	0.29	0.68	0.74	0.40
Mg	-	-	-	-	0.06	-	0.06	0.03	0.36	0.56
Ca	-	0.01	0.02	-	0.01	0.02	0.31	0.03	0.19	0.20
Ba	-	0.26	0.43	0.01	0.75	0.65	0.17	0.39	0.17	0.12
Sr	-	0.01	0.01	-	0.01	0.01	0.16	0.24	0.07	0.04
K	-	0.74	0.48	-	0.09	0.21	0.18	0.23	0.10	0.03
Na	0.01	0.06	0.08	-	0.03	0.03	0.39	0.13	0.41	0.50
Ce	-	-	-	-	-	-	-	-	-	-
Zn	-	-	-	0.01	0.02	-	0.04	0.01	0.02	0.02
Ni	-	-	-	-	0.03	-	-	0.01	-	-
Total	1.02	8.78	8.68	1.01	8.58	8.57	8.87	8.81	9.01	8.99

n.d. = none detected.

TABLE III (cont)

	Pyrolusite(?) 2854	Ferrian Hollandite 2854			Hollandite 2947			Hollandite 2955		
SiO_2	0.97	0.85	1.20	2.49	0.47	0.94	0.55	0.39	0.37	0.20
TiO_2	0.43	0.68	1.00	0.62	0.39	1.06	0.48	0.67	0.41	0.21
MnO_2	84.08	75.98	74.21	62.58	82.02	72.95	77.06	81.03	77.58	78.69
Al_2O_3	1.20	1.47	1.67	1.55	0.42	0.65	0.60	0.62	0.41	0.14
Fe_2O_3	2.92	4.44	6.53	18.28	2.40	4.49	1.94	3.58	2.71	1.96
MgO	n.d.	0.38	n.d.	0.06	0.09	0.20	0.21	0.20	0.92	2.18
CaO	0.35	0.37	0.36	0.37	0.73	0.94	1.16	0.35	0.93	1.20
BaO	1.46	5.59	9.02	6.06	5.40	5.66	9.60	4.28	4.71	4.22
SrO	n.d.	0.24	0.43	0.21	1.18	0.84	1.21	1.03	1.20	1.15
K_2O	n.d.	0.09	0.20	0.23	3.49	2.47	0.47	3.75	1.71	0.40
Na_2O	n.d.	n.d.	0.14	n.d.	0.42	0.40	0.58	0.53	0.86	1.51
CeO_2	*	n.d.	n.d.	n.d.	n.d.	n.d.	n.d.	n.d.	n.d.	n.d.
ZnO	n.d.	0.12	0.11	n.d.	0.16	n.d.	n.d.	n.d.	n.d.	n.d.
NiO	n.d.	0.13	n.d.	n.d.	n.d.	n.d.	n.d.	n.d.	n.d.	n.d.
Total	91.41	90.34	94.87	92.45	97.17	90.60	93.86	96.43	91.81	91.86
	Stoich (O=2)	Stoich (O=16)	Stoich (O=16)	Stoich (O=16)	Stoich (O=16)	Stoich (O=16)	Stoich (O=16)	Stoich (O=16)	Stoich (O=16)	Stoich (O=16)
Si	0.02	0.11	0.16	0.34	0.06	0.13	0.07	0.05	0.05	0.03
Ti	0.01	0.07	0.10	0.06	0.04	0.11	0.05	0.06	0.04	0.02
Mn	0.93	7.06	6.76	5.81	7.26	6.92	7.19	7.17	7.19	7.21
Al	0.02	0.23	0.26	0.25	0.06	0.11	0.10	0.09	0.06	0.02
Fe	0.04	0.45	0.65	1.85	0.23	0.46	0.20	0.35	0.27	0.20
Mg	-	0.08	0.01	0.01	0.02	0.04	0.04	0.04	0.18	0.43
Ca	0.01	0.05	0.05	0.05	0.10	0.14	0.17	0.05	0.13	0.17
Ba	0.01	0.29	0.47	0.32	0.27	0.30	0.51	0.22	0.25	0.22
Sr	-	0.02	0.03	0.02	0.09	0.07	0.09	0.08	0.09	0.09
K	-	0.01	0.03	0.04	0.57	0.43	0.08	0.61	0.29	0.07
Na	-	-	-	-	0.11	0.11	0.15	0.13	0.22	0.39
Ce	-	-	-	-	-	-	-	-	-	-
Zn	-	0.01	0.01	-	0.01	-	-	-	-	-
Ni	-	0.01	-	-	-	-	-	-	-	-
Total	1.04	8.39	8.53	8.75	8.82	8.82	8.65	8.85	8.77	8.85

*May be present $\leq$0.5%. Not measured quantitatively.

zeolitic coatings may not be continuous over the entire interval, the gaps usually correlate with a marked decrease in fracture abundance. The first zeolite interval below the SWL is continuous with the lower zeolitic interval above the SWL. The second interval of zeolite-lined fractures occurs in the argillic and zeolitic zones of the Prow Pass Member, the bedded tuff below it, and the uppermost Bullfrog Member. Figure 2 shows a gap in the zeolite fracture fill in the lower Prow Pass Member that correlates with a gap in the sampling and is a result of the scarcity of fractures intersected by the drill hole over this interval. Trace amounts of mordenite are found in fractures immediately below this zeolitic interval in devitrified tuff at 2273 and 2279 ft. Mordenite and clinoptilolite may also occur in trace amounts at 2656 ft but were only tentatively identified from SEM images. The third interval of zeolite-lined fractures occurs from 2695 ft to the bottom of the hole. The top of this interval correlates with the occurrence of zeolitic and argillic tuff, but zeolites in fractures continue below the interval of zeolitic rock matrix. The two apparent gaps in zeolite fracture fill in this interval may again be caused by a paucity of filled fractures, though the few fractures that do exist in these gaps contain minerals other than zeolites (Fig. 2). A sampling volume larger than a single drill core would be needed to determine if these gaps in zeolite occurrence are real. Fractures in a deeper hole (such as USW G-1) will be studied to determine what relationship, if any, exists between fracture and matrix mineralogy in the deeper alteration zones.

Mordenite is the principal zeolite in all the fractures. It forms cryptocrystalline coatings of long matted filaments or shorter bristly filaments, usually with small grains of clinoptilolite and/or quartz and possibly potassium feldspar on or embedded in the mats (Figs. 3 and 4). It is often difficult to determine on the SEM images whether the small grains are detrital fragments derived from drilling that became embedded in the mordenite mats or anhedral grains that grew with or on the mordenite. Slickensides are visible on some mordenite mats.

Clinoptilolite is identified in many XRD patterns. Small (<10-μm) anhedral grains embedded in the mordenite mats were tentatively identified as clinoptilolite on the basis of qualitative EDS analysis on the SEM (Fig. 4). SEM images suggest that at least some of these were coprecipitated with the mordenite. Large euhedral crystals (0.1-0.2 mm) of clinoptilolite are not common below the SWL; they occur under cristobalite and manganese oxides in

Fig. 3.
SEM image of long fibers of mordenite in fracture from 1788 ft.

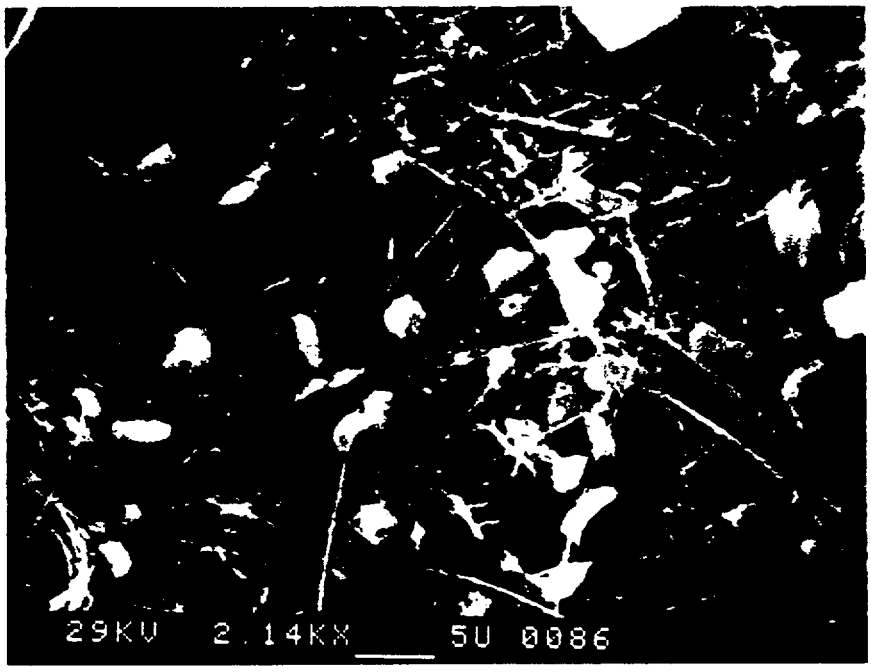

Fig. 4.
SEM image of shorter fibers of mordenite with grains that are probably clinoptilolite. From 2062 ft.

fractures at 2099 ft (Figs. 5 and 6) and under mordenite in fractures at 2126 and 2698 ft (Figs. 7 and 8). Unlike the small anhedral grains, these euhedral clinoptilolites formed early in the depositional sequence. Electron microprobe analyses of these euhedral clinoptilolites as well as the fine-grained clinoptilolite and mordenite that occur with them are given in Table II. Figure 9(a) is a ternary diagram of their cation compositions. The mordenite plots in the same region as mordenite from fractures above the SWL (Carlos 1985). Comparison of fracture clinoptilolite compositions with rock matrix clinoptilolite compositions plotted on Fig. 9(b) shows that they are similar, though fracture clinoptilolites from 2698 ft are more sodic than matrix clinoptilolite from a similar depth (2738 ft). None of the samples have been heated to determine mineral stability and possible presence of heulandite instead of clinoptilolite (Mumpton 1960), but the Si:Al ratios are typical of clinoptilolite rather than heulandite (Boles 1972).

Cristobalite occurs alone in fractures between 2125 and 2140 ft. The presence of pure cristobalite in fractures in an interval of zeolite-lined fractures is unusual. It was thought that perhaps the tuff over the entire interval might be rich in cristobalite, but XRD analyses in this interval do not indicate any cristobalite in the rock matrix (Bish and Vaniman 1985). Cristobalite also occurs under or over euhedral clinoptilolite in fractures with multiple coatings, at least down to 2700 ft depth; it has not been identified in XRD patterns of fracture minerals below that depth. It is seen on few SEM images of open fractures from the saturated zone (Fig. 5) and can be seen in some thin sections (Figs. 6 and 8).

Quartz is nearly ubiquitous in XRD patterns of fractures that have any coating at all. It is not readily identifiable in SEM images of fractures in the Prow Pass Member (above 2237 ft) but is visible in several forms in deeper fractures. Small amounts of quartz identified on Table I may be a result of contamination during scraping for XRD analysis. Anhedral grains also occur embedded in mordenite mats and some may be fragments from drilling. Below 2850 ft quartz appears as late-stage, tiny (10-μm) ellipsoidal crystals on mordenite (Fig. 10) and with manganese oxides. In at least one of these fractures, quartz also occurs as earlier etched crystals under the mordenite (Fig. 11). An unusual tabular quartz with silica overgrowths occurs with feldspar and minor cristobalite in a fracture at 2344 ft. The fracture is in a vapor-phase zone, and the minerals in the fracture are interpreted as

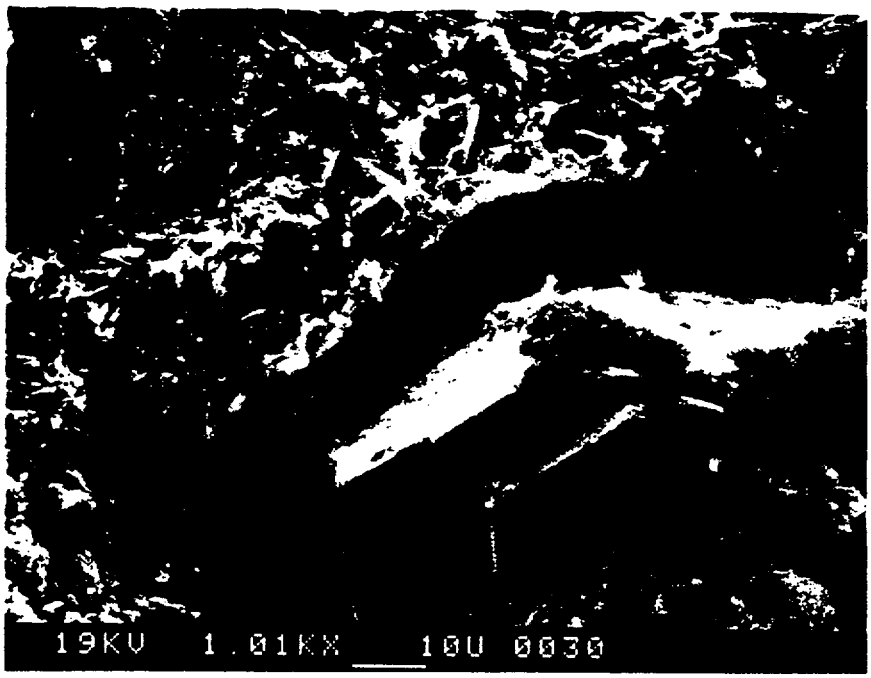

Fig. 5.
SEM image of clinoptilolite under cristobalite and hollandite. From 2099 ft.

Fig. 6.
Photomicrograph of fracture from 2099 ft. Fracture is lined with clinoptilolite (white) that is rimmed with cristobalite (beige) and filled with pyrolusite and hollandite intergrown with mordenite (and cristobalite?). Photo width is 1 mm.

Fig. 7.
SEM image of mordenite over clinoptilolite in fracture from 2126 ft.

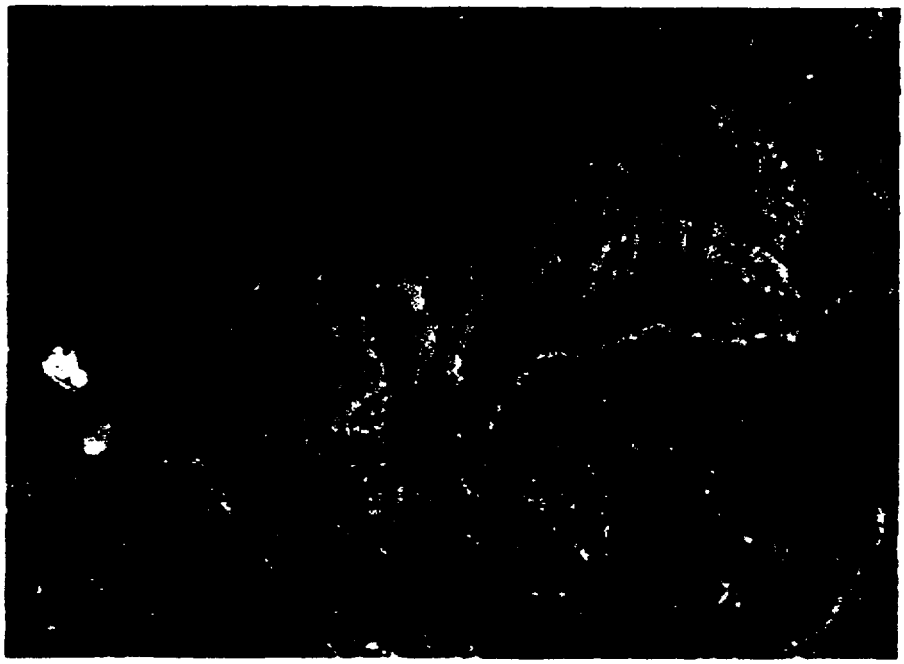

Fig. 8.
Photomicrograph of fracture from 2698 ft. Fracture is rimmed with fine-grained mordenite, then (yellow) cristobalite, then coarser euhedral clinoptilolite and filled with coarse mordenite. Width of photo is 1 mm.

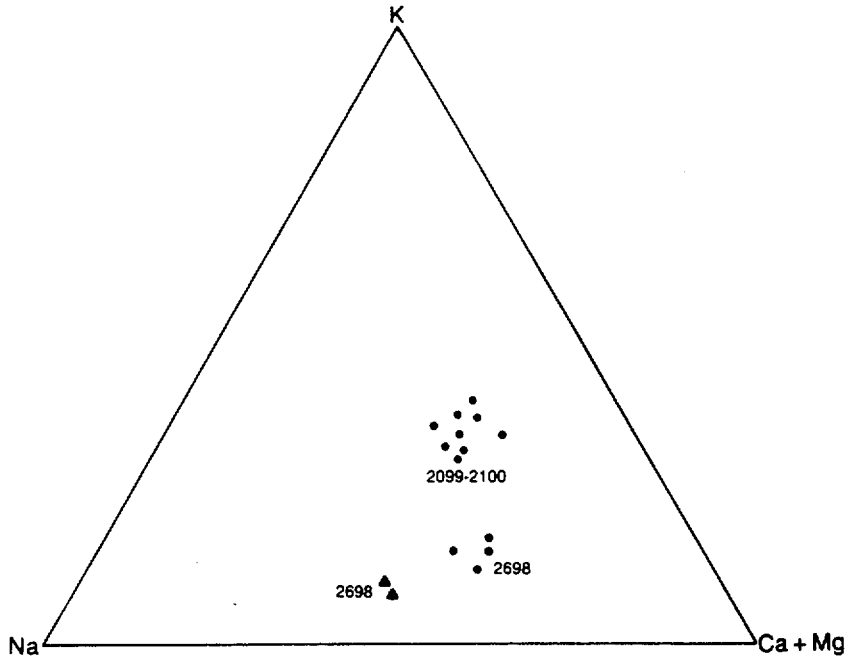

Fig. 9(a).
Na-K-Ca+Mg ternary diagram of fracture zeolites below the SWL in USW G-4.

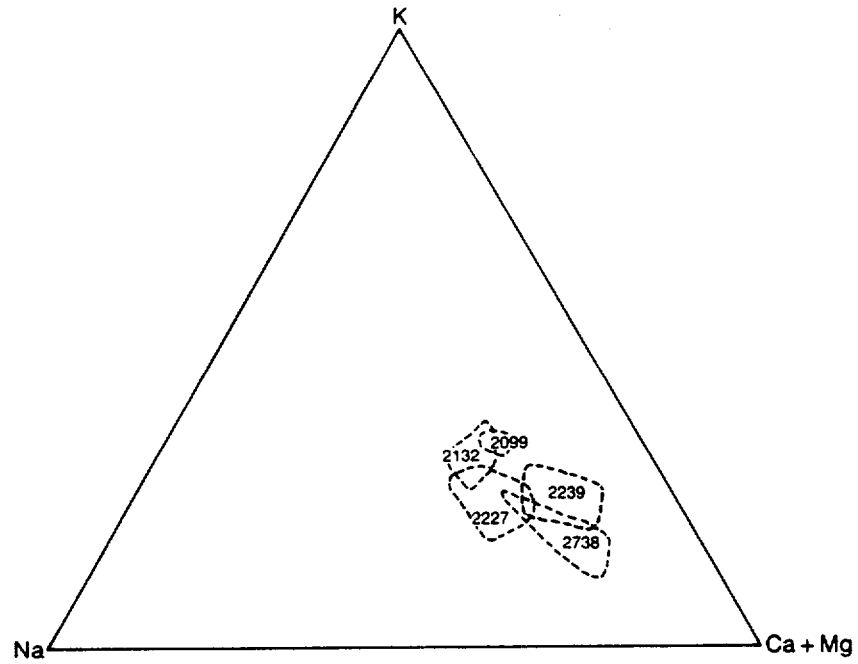

Fig. 9(b).
Na-K-Ca+Mg ternary diagram showing fields of composition for rock matrix clinoptilolites below the SWL in USW G-4. Data from this study (2099 ft) and Broxton et al. 1986b. Numbers are sample depths.

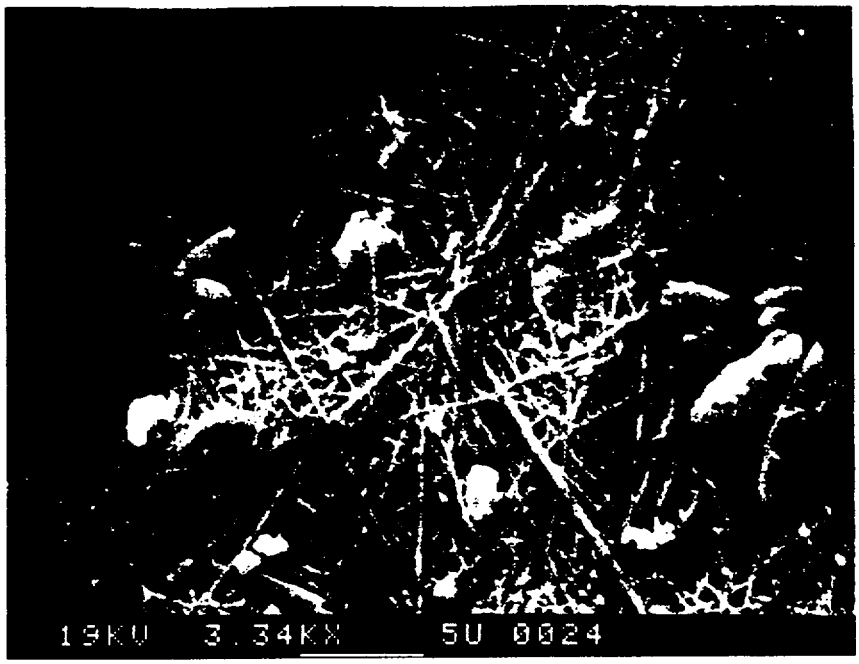

Fig. 10.
SEM image of ellipsoidal quartz on mordenite from fracture at 2904 ft.

Fig. 11.
SEM image of etched quartz partially covered with mordenite, 2904 ft.

vapor-phase filling because of the bleached zone surrounding the fracture and the similarity of the coating to lithophysal-type fractures in the unsaturated zone (Carlos 1985). Both the bleached zone and the fracture minerals in the unsaturated zone are much fresher than they are in this fracture, but that would be expected if this fracture filling formed during the cooling of the Crater Flat Tuff. As this fracture is the only one of its type observed below the SWL, the identification is tentative, but the similarity in appearance is striking. The morphology of the quartz suggests it may originally have crystallized as tridymite, but the XRD pattern indicates quartz is the principal silica mineral now. Another early occurrence of quartz that may be a composite crystal or may have inverted from an earlier silica polymorph (also tridymite?) is the "asparagus-tip" quartz at 2656 ft (Fig. 12). It resembles the quartz dipyramid shown in Finkelman (1975), but does not have such sharp terminations, and is partially coated by tiny clinoptilolite and mordenite; all underlie calcite. Large (10-40 μm) euhedral quartz crystals underlie hollandite at 2578 ft (Fig. 13), but they may not be as early as the etched crystals in the fracture at 2904 ft. Small, multiply terminated quartz crystals occur in several fractures with hollandite (Fig. 14), either with or instead of the ellipsoidal crystals mentioned above.

Alkali feldspar, usually potassium feldspar, is indicated on the XRD patterns of many fractures but does not appear as euhedral crystals on SEM images. In some cases, for instance the fractures at 1991, 2954, and 2967 ft, the feldspar is probably part of the rock matrix that became intergrown with the zeolite or manganese fracture fill. Feldspar is commonly intergrown with quartz in the lithophysal-type fractures above the SWL and probably is also in the fracture at 2343 ft. The only possible feldspar identified on SEM images for that fracture was in small grains or fragments that may have been detrital drilling fragments rather than original coating. This was also the case for similar fractures above the SWL. Anhedral grains embedded in mordenite mats are tentatively identified as potassium feldspar on the basis of qualitative EDS analysis. Unlike all the other fracture-coating minerals, no distinct layer of feldspar has been identified in any fracture.

Smectite clays occur in few fractures but are relatively abundant where they do occur (Table I). The only sample with sufficient material to allow clay separation (fracture at 1991 ft) contained an unidentifiable amount of argillic matrix in the scraped fracture coating so that the actual fracture

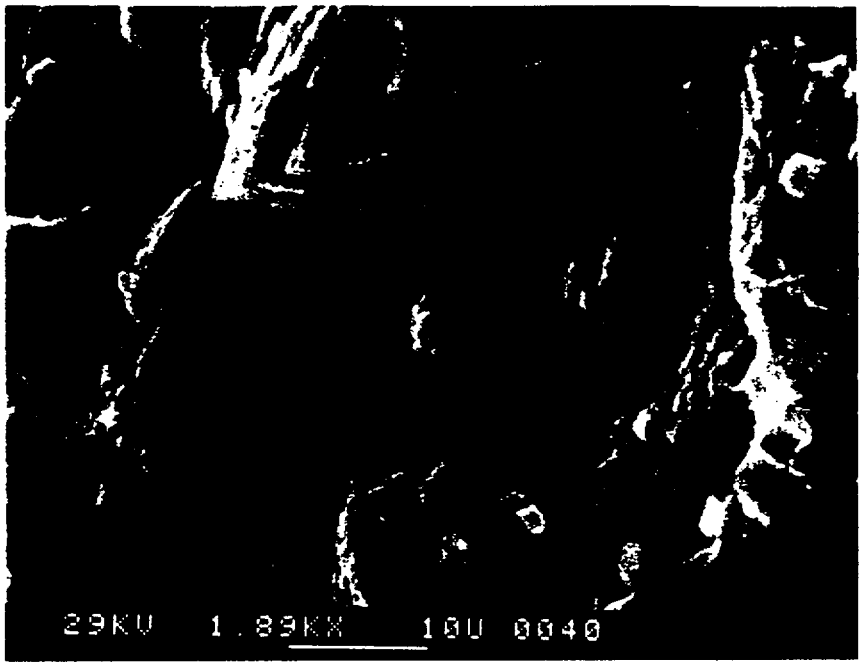

Fig. 12.
SEM image of "asparagus tip" quartz with tiny clinoptilolite and a few mordenite hairs coating the quartz. Calcite (not shown) later filled fracture. From 2656 ft.

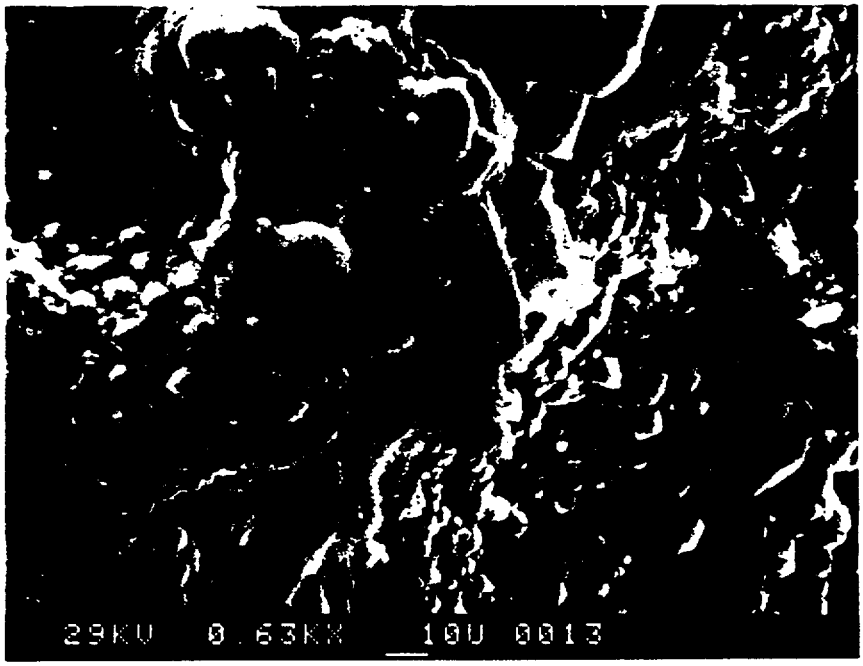

Fig. 13.
SEM image of euhedral quartz under hollandite (fibers) in fracture from 2578 ft.

Fig. 14.
SEM image of multiply terminated quartz with hollandite from fracture at 2947 ft.

coat may or may not have contained any clay. The results of the glycolated clay separate for that sample indicated randomly interstratified smectite/illite with at least 90% smectite layers. Interferences with higher order peaks preclude more precise determination of the amount of smectite.

IV. OCCURRENCE OF CALCITE

Calcite occurs in fractures over a very limited depth range in the saturated zone of USW G-4 and has a discontinuous distribution over that range (Fig. 2). Calcite occurs with manganese oxide minerals, and in some fractures with quartz, in the lower Bullfrog Member of the Crater Flat Tuff, from 2578 to 2660 ft. It is the youngest mineral in the depositional sequence but may be intergrown with manganese oxide minerals (Figs. 15 and 16). It occurs alone in fractures in the upper Tram Member and in the lower part of the bedded interval between the Bullfrog and the Tram, from 2751 to 2761 ft.

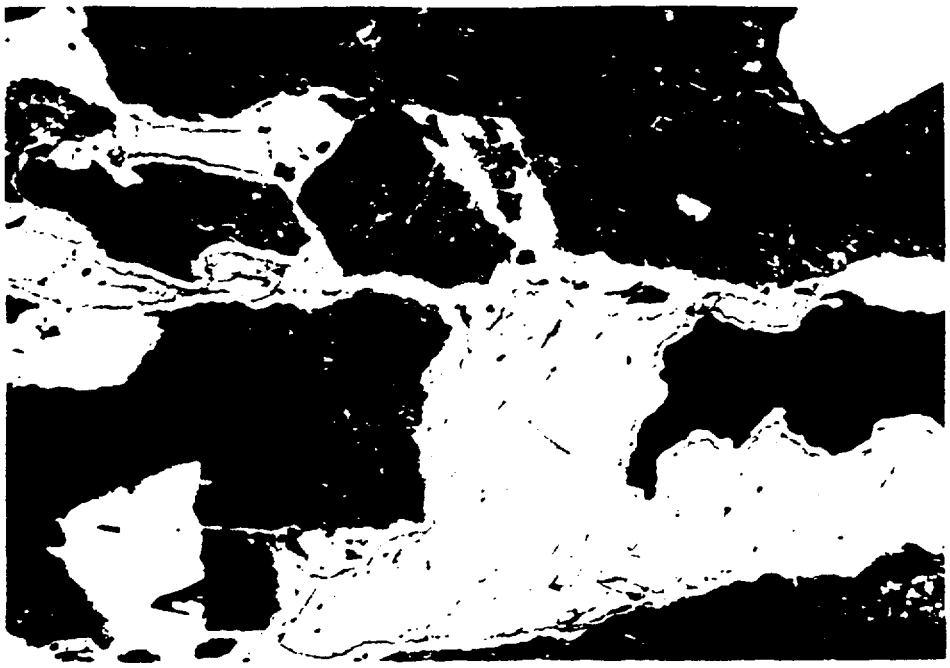

Fig. 15.
Photomicrograph of fracture from 2620 ft. Silica forms rims; pure calcite and calcite intergrown with manganese oxide (black) fill fracture. Photo width is 2.5 mm.

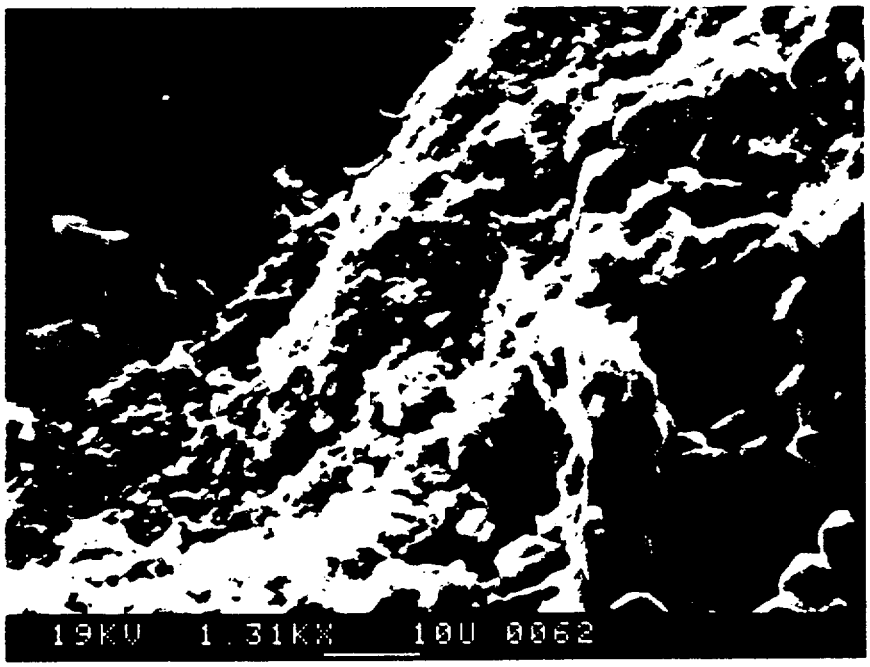

Fig. 16.
SEM image showing calcite over hollandite coating quartz at 2578 ft.

V. MANGANESE OXIDE MINERALS

Manganese oxide minerals in fractures in the saturated zone of USW G-4 have limited distribution (Fig. 2) but form abundant thick coatings where they occur. Unlike the sparse manganese oxides in the Topopah Spring Member of the Paintbrush Tuff above the SWL, the larger patches of which are lithiophorite, the continuous manganese oxide coatings found in the Crater Flat Tuff are cryptomelane-family minerals (cryptomelane and hollandite) and, in some intervals, pyrolusite. Within a single fracture the manganese oxides often have more than one composition and sometimes form more than one mineral. Manganese minerals were identified by XRD in samples with sufficient material. Representative chemical compositions as determined by microprobe are listed in Table III. None of these compositions represents a unique analysis; even when three or four compositions are given for the same sample, each one represents a group of three or four analyses on different grains.

The manganese oxide minerals pyrolusite and possibly cryptomelane occur along a shear zone at 1990 ft where they surround or replace pulverized zeolitic rock matrix and fill in voids. Most of the oxides are too fine-grained and intergrown with rock matrix to analyze, but two distinct compositions were obtained from manganese minerals filling voids (Table III).

Pyrolusite and hollandite fill several subhorizontal fractures between 2093 and 2100 ft. These fracture coatings are a thick sooty black, with tufts of acicular hollandite up to 0.4 mm across. SEM images show that hollandite was deposited on cristobalite and either preceded mordenite or was co-deposited (Figs. 5 and 17). Hollandite and pyrolusite are both seen in thin sections of fractures previously lined with clinoptilolite and cristobalite (Fig. 18), but an earlier deposit of manganese oxide lined some of the fractures before clinoptilolite deposition. A later mordenite-filled fracture cuts one of these horizontal fractures, coating the trace of at least some of the manganese oxides and clinoptilolite.

The manganese minerals hollandite or cryptomelane form continuous black coatings on the surface of fractures from 2565 to 2680 ft depth, usually over quartz and under calcite. They all have similar acicular or stubby filiform morphology as seen in SEM images, but they have very different minor element chemistry, even within the same sample (Table III).

Manganese oxides occur at the base of a discolored zone at 2814 ft. A vertical fracture containing cryptomelane intersects it, but the manganese

Fig. 17.
SEM image of hollandite (rods) with mordenite. From 2099 ft.

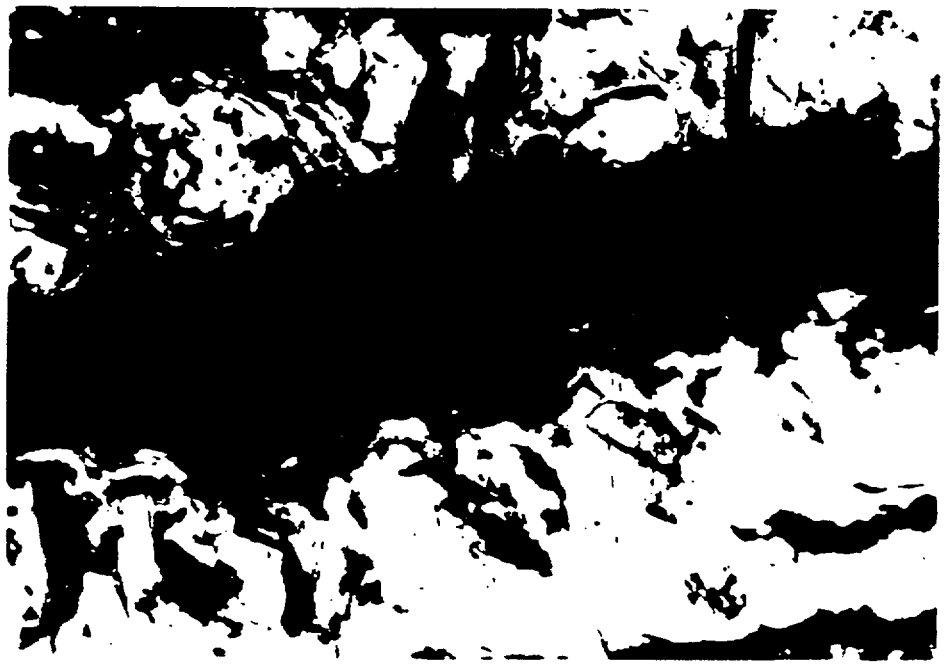

Fig. 18.
Photomicrograph of pyrolusite (round gray mass) and hollandite (smaller gray rods) filling clinoptilolite-lined fracture from 2099 ft. Photo width is 0.5 mm.

minerals in the broader zone are too fine grained to analyze. From 2850 to 3000 ft manganese oxide coatings often occur with red-brown hematite staining and are often slickensided. The manganese minerals are hollandite and cryptomelane with several compositions as in the interval above (Table III), but the coatings are less continuous and the individual crystals are smaller. The manganese oxides are frequently intergrown with spherulites formed during devitrification of the tuff (Fig. 19).

VI. SUMMARY OF FRACTURE-MINERAL PARAGENESIS AND DISCUSSION

Although fracture minerals below the SWL occur in several assemblages, some observations can be made on the sequence of deposition, and some tentative conclusions can be made on the age of some of the fracture minerals. Some quartz is definitely early. The fracture coating at 2344 ft with tabular quartz that is overgrown with crusts of fine-grained silica is probably a vapor-phase deposit and may originally have been tridymite, which has inverted to quartz. It resembles in morphology and mineralogy the lithophysal-type fractures in the unsaturated zone. The distinctive asparagus-tip quartz seen in fractures at 2656 ft formed early in the sequence of those fractures. In another fracture, large euhedral quartz appears to have been etched by later fracture fluids and overgrown with mordenite. Unetched quartz coated by manganese oxides may also have formed very early. Euhedral clinoptilolite is the earliest zeolite mineral and is observed under mordenite and/or manganese oxides. At 2099 ft clinoptilolite underlies cristobalite. There are few occurrences of large ($\geq$0.1-mm) clinoptilolites below the SWL; they are much more abundant in the unsaturated zone. It is possible that those in the Crater Flat Tuff formed before the deposition of the Tuffs of Calico Hills and the Paintbrush Tuff and the subsequent zeolitic alteration of the entire tuff sequence. Cristobalite is often an early fracture lining, as seen in thin section, but most of it may be from a later alteration phase than are the above-mentioned quartz and the large euhedral clinoptilolite.

Manganese oxides occur in more than one generation. In addition to the evidence of early and later manganese oxides in a single sample, the chemistry both within a single sample and between samples is markedly different. Zones of manganese oxide deposition in fractures are separated by barren zones. All of these suggest that manganese oxides were deposited by different fluids at

Fig. 19.
Photomicrograph of manganese oxides intergrown with spherulites at edge of fracture from 2947 ft. Photo width is 0.5 mm.

different times as well as by fluids that were separated vertically. There does not seem to be a systematic change in the manganese oxide chemistry with depth. Manganese oxides were deposited both before and after clinoptilolite and cristobalite, before or with mordenite and calcite.

Mordenite is the principal zeolite in fractures. This is in contrast to the zeolitic rock matrix wherein clinoptololite is more abundant than mordenite. Mordenite forms thicker, coarser grained and more continuous coatings below the SWL than above and is mostly confined to zeolitic tuff intervals. The occurrence of zeolites in fractures correlates strongly with their occurrence in the rock matrix in the upper two intervals of zeolitic Crater Flat Tuff. In addition, the compositions of whole rock and fracture-lining clinoptilolites at corresponding depths in these two intervals (including that portion of the upper interval that is in the Tuffs of Calico Hills above the present SWL) are markedly similar. Although the number of analyzed samples provides insufficient basis for more than tentative conclusions, these correlations suggest that the fracture and rock matrix zeolites may have formed at the same time from the same solutions. The

vertical correlation of zeolitic tuff and fractures suggests that the flow may have been lateral through porous intervals in the tuff rather than vertical through fractures. The difference in relative abundances of mordenite and clinoptilolite between the rock matrix and fractures is probably controlled by the Si:Al ratio in the fluids; a drop in Al activity would cause the deposition of mordenite preferentially to clinoptilolite. This drop in Al activity could be caused simply by the fluid moving laterally from the rock matrix, where glass containing Al was being actively dissolved, to the fracture, where the fluid was not being buffered by glass dissolution. Vertical movement of fluid in the fractures during zeolitization is not required to explain the presence of mordenite rather than clinoptilolite and is only indicated where zeolites occur in fractures in nonzeolitic matrix. Mordenite is difficult to analyze by microprobe because of its grain size, but the single sample analyzed from below the SWL (an early rind of fine-grained mordenite) is nearly identical in composition to the single analyzed sample above the SWL. It is, however, the earliest coating in a multistage fracture filling, and it is doubtful both mordenites are from the same fluid. The clinoptilolite from the same depth (2698 ft), which is in the lowest zeolitic interval in this drill hole, is apparently more sodic than are rock matrix clinoptilolites from the same zeolitic interval, but the reported Na values for rock matrix zeolites may be low because of the difficulty in analyzing small zeolite grains. The fracture clinoptilolite precedes a coarse-grained mordenite that forms a solid filling in the clinoptilolite-lined fracture but could not be analyzed by microprobe. Mordenite occurs in fractures below the lowest zeolitic tuff in this drill hole, suggesting that the fluid flow paths and/or timing of zeolitization may have been different at this depth than at shallower intervals below the SWL and that the fluid flow paths may have included vertical flow through fractures. Small grains of clinoptilolite and quartz (identified by SEM) lying on or embedded in the mordenite probably formed at least slightly later than the mordenite, though some may have formed with it.

Calcite is the youngest mineral in most fractures where it occurs. It is intergrown with manganese in one sample, but the genetic relationship has not been determined; the apparent intergrowth may be calcite deposition between pre-existing hollandite rods.

VII. CONCLUSIONS

There probably were two separate periods of silicate deposition in fractures. The first occurred after deposition of the Crater Flat Tuff and before deposition of the later tuffs. During this time lithophysal-type fractures formed containing quartz (tridymite?), cristobalite, and feldspar. Clinoptilolite and possibly the early fine-grained mordenite may have formed in some fractures.

After deposition of the Tuffs of Calico Hills and the Paintbrush Tuff, major zeolitization occurred in the entire pile of tuffs. Mordenite and possibly some euhedral clinoptilolite formed in the fractures of the zeolitized tuffs at this time, and perhaps the tiny grains of clinoptilolite and quartz were either codeposited or formed soon after. Broxton et al. (1986a) conclude that the major rock matrix zeolitization episode was between 13 and 11 m.y. ago. The correlation between zeolites in fractures and zeolitic rock matrix in most of the saturated zone suggests that most of the fracture zeolites also formed during this episode.

Manganese oxides have a complex history and probably were deposited over a longer period of time than any other fracture mineral. Most seem to have been deposited before the mordenite. Calcite is the youngest mineral in those few fractures where it occurs. The relationships between the fracture minerals and the correlation between fracture minerals and tuff mineralogy suggest that most of the fracture mineralization was complete by 11 m.y. ago. There is no evidence that dates the calcite and the small grains of quartz, potassium feldspar, and clinoptilolite, except that they came after most of the fracture mineralization.

ACKNOWLEDGMENTS

The author wishes to thank D. Bish, D. Krier, C. Grigsby, and C. Duffy for their thought-provoking discussions and D. Bish and D. Krier for critically reading this manuscript and suggesting improvements.

REFERENCES

Bence, A. E., and A. L. Albee, 1968, Empirical correction factors for electron microanalysis of silicates and oxides. J. Geol. 76, 382-403.

Bish, D. L., F. A. Caporuscio, J. F. Copp, B. M. Crowe, J. D. Purson, J. R. Smyth, and R. G. Warren, 1981, Preliminary stratigraphic and petrologic characterization of core samples from USW-G1, Yucca Mountain, Nevada. A. C. Waters and P. R. Carroll, eds., Los Alamos National Laboratory report LA-8840-MS.

Bish, D. L., and D. T. Vaniman, 1985, Mineralogic summary of Yucca Mountain, Nevada. Los Alamos National Laboratory report LA-10543-MS.

Boles, J. R., 1972, Composition, optical properties, cell dimensions, and thermal stability of some heulandite group zeolites. Am. Mineral. 57, 1463-1493.

Broxton, David E., and Barbara Arney Carlos, 1986, Zeolitic alteration and fracture fillings in silicic tuffs at a potential nuclear waste repository, Yucca Mountain, Nevada, USA. Extended Abstract in Fifth International Water-Rock Interaction Symposium, Reykjavik, Iceland, August 8-17, 1986, p. 88-91.

Broxton, David E., David L. Bish, and Richard G. Warren, 1986a, Distribution and chemistry of diagenetic minerals at Yucca Mountain, Nye County, Nevada. Clays Clay Miner. (in press).

Broxton, David E., Richard G. Warren, Roland C. Hagan, and Gary Luedemann, 1986b, Chemistry of diagenetically altered tuffs at a potential nuclear waste repository, Yucca Mountain, Nye County, Nevada. Los Alamos National Laboratory report LA-10802-MS.

Byers, F. M., Jr., W. J. Carr, P. Orkild, W. D. Quinlivan, and K. A. Sargent, 1976, Volcanic suites and related calderas of Timber Mountain-Oasis Valley Caldera Complex, Southern Nevada. US Geol. Surv. Prof. Paper 919.

Carlos, B. Arney, 1985, Minerals in fractures of the unsaturated zone from drill core USW G-4, Yucca Mountain, Nye County, Nevada. Los Alamos National Laboratory report LA-10415-MS.

Carr, W. J., F. M. Byers, Jr., and P. P. Orkild, 1986, Stratigraphic and volcano-tectonic relations of Crater Flat Tuff and some older volcanic units, Nye County, Nevada Test Site. US Geol. Surv. Prof. Paper 1323.

Carr, W. J., 1974, Summary of tectonic and structural evidence for stress orientation at the Nevada Test Site. US Geol. Surv. Open-file report 74-176.

Finkleman, Robert B., 1975, Perched silica minerals on mordenite fibers. Jour. Research U.S. Geol. Survey, 3, no. 2, p. 197-202.

Graham, J., C. R. M. Butt, and R. B. W. Vigers, 1984, Sub-surface charging, a source of error in microprobe analysis. X-Ray Spectrom. 1(3), 126-133.

Lipman, P. W., R. L. Christiansen, and J. T. O'Connor, 1966, A compositionally zoned ash-flow sheet in southern Nevada. US Geol. Surv. Prof. Paper 524-F, 47 p.

Mumpton, F. A., 1960, Clinoptilolite redefined. Am. Mineral. 45, 351-369.

Scott, R. B., R. W. Spengler, S. Diehl, A. R. Lappin, and M. P. Chornack, 1983, Geologic character of tuffs in the unsaturated zone at Yucca Mountain, southern Nevada: in J. W. Mercer, P. S. L. Rao, and I. W. Irvine, Eds., Role of the Unsaturated Zone in Radioactive and Hazardous Waste Disposal. Ann Arbor Science, Ann Arbor, Michigan, p. 289-335.

Spengler, R. W., and M. P. Chornack, 1984, Stratigraphic and structural characteristics of volcanic rocks in core hole USW G-4, Yucca Mountain, Nye County, Nevada, section on geophysical logs by D. C. Muller and J. E. Kibler. US Geol. Surv. Open-file report 84-789.

☆ U.S. GOVERNMENT PRINTING OFFICE 1987—773-103/40052